Wildfire Smoke Observations in the Western United States from the Airborne Wyoming Cloud Lidar during the BB-FLUX Project. Part II: Vertical Structure and Plume Injection Height

MIN DENG,[a,b] RAINER M. VOLKAMER,[c] ZHIEN WANG,[b,c] JEFFERSON R. SNIDER,[a] NATALIE KILLE,[c] AND LEIDY J. ROMERO-ALVAREZ[c]

[a] *Department of Atmospheric Science, University of Wyoming, Laramie, Wyoming*
[b] *Laboratory of Atmosphere and Space Physics, University of Colorado Boulder, Boulder, Colorado*
[c] *Department of Atmospheric and Oceanic Sciences, University of Colorado Boulder, Boulder, Colorado*

(Manuscript received 30 June 2021, in final form 7 January 2022)

ABSTRACT: The western U.S. wildfire smoke plumes observed by the upward-pointing Wyoming Cloud Lidar (WCL) during the Biomass Burning Fluxes of Trace Gases and Aerosols (BB-FLUX) project are investigated in a two-part paper. Part II here presents the reconstructed vertical structures of seven plumes from airborne WCL measurements. The vertical structures evident in the fire plume cross sections, supported by in situ measurements, showed that the fire plumes had distinct macrophysical and microphysical properties, which are closely related to the plume transport, fire emission intensity, and thermodynamic structure in the boundary layer. All plumes had an injection layer between 2.8 and 4.0 km above mean sea level, which is generally below the identified boundary layer top height. Plumes that transported upward out of the boundary layer, such as the Rabbit Foot and Pole Creek fires, formed a higher plume at around 5.5 km. The largest and highest Pole Creek fire plume was transported farthest and was sampled by University of Wyoming King Air aircraft at 170 km, or 2.3 h, downwind. It was associated with the warmest, driest, deepest boundary layer and the highest wind speed and turbulence. The Watson Creek fire plume intensified in the afternoon with stronger CO emission and larger smoke plume height than in the morning, indicating a fire diurnal cycle, but some fire plumes did not intensify in the afternoon. There were pockets of relatively large irregular aerosol particles at the tops of plumes from active fires. In less-active fire plumes, the WCL depolarization ratio and passive cavity aerosol spectrometer probe mass mean diameter maximized at a height that was low in the plume.

KEYWORDS: Aircraft observations; In situ atmospheric observations; Lidars/lidar observations; Remote sensing; Biomass burning; Wildfires

1. Introduction

Recently, wildfires have become more active and aggressive in North America as a result of increases in temperature, drought, and fuel load (Kitzberger et al. 2007; Littell et al. 2009; Westerling 2016). The aerosol particles and trace gases emitted from wildfires cause negative impacts on air quality and are harmful to people and the environment (Landis et al. 2018; Meng et al. 2019). These emissions are variable and depend on for example fire intensity and plume injection height. The latter influences smoke transport and dispersion. Wildfire smoke can be transported over continental and transcontinental distances (Damoah et al. 2004; Derwent et al. 2004; Duck et al. 2007; Lutsch et al. 2016, 2019). Therefore, an extremely important component in modeling wildfire emissions and thus predicting air quality impact is knowledge of plume height and plume rise from wildfires.

Labonne et al. (2007) found from *Cloud–Aerosol Lidar and Infrared Pathfinder Satellite Observations* (*CALIPSO*) lidar measurements that wildfire smoke is often confined to the planetary boundary layer (PBL), and is rarely lofted higher than the PBL top. In contrast, Kahn et al. (2008) and Val Martin et al. (2010), using data from the Multiangle Imaging SpectroRadiometer (MISR) instrument on board the NASA *Terra* satellite, indicated that approximately 5%–18% of the plumes reached the free troposphere over Alaska and the Yukon Territories (Canada) in 2004; the altitude of the observed plumes ranged from a few hundred meters to 4.5 km above the terrain. The height of plumes from the Tropospheric Monitoring Instrument (TROPOMI; Griffin et al. 2020) are in reasonable agreement with MISR, but the MISR-derived values represent the top of a smoke plume whereas the TROPOMI values are derived by profiling downward, from the top of the plume, into the underlying smoke plume layers. The disparity between the *CALIPSO* lidar, MISR, and TROPOMI (Kahn et al. 2008) highlights the complexities involved when collecting representative fire plume height data over a variety of locations.

The factors modulating where plumes level off and start to advect horizontally (i.e., the smoke injection height) remain poorly understood and underobserved. Fire intensity, measured as fire radiative power (FRP), modulates the injection height (Val Martin et al. 2012; Peterson et al. 2015). Forest fire emissions typically follow a diurnal cycle with a decrease in emissions and intensity during the night when fuel moisture, wind, and other ambient atmospheric conditions are less favorable, and with an increase through the day until the late afternoon (Ye et al. 2021; Zheng et al. 2021). On the other hand, fires may modify the structure of the PBL by reducing the insolation (Youn et al. 2011; Lareau and Clements 2015;

Corresponding author: Min Deng, mdeng2@uwyo.edu

DOI: 10.1175/JTECH-D-21-0093.1

Kochanski et al. 2019). Thus, stable layers and mixing heights near fires may differ from those resolved by forecast models and observed by regional radiosonde networks. Meteorological observations near wildfires are rare, especially when compared with the established observational record for other atmospheric processes (e.g., convective storms). This observational deficit likely stems from the considerable logistical and safety challenges associated with sampling in the near-fire environment (Viegas 1998).

These observational deficits, coupled with uncertainties in plume-rise models, led Val Martin et al. (2012) to conclude that direct field measurements of fire and smoke plume properties are required to produce the next major advance in plume modeling. During the Biomass Burning Fluxes of Trace Gases and Aerosols (BB-FLUX) project, a suite of active remote sensing measurements, in situ aerosol and trace gas measurements, and a flexible airborne platform for vertical meteorological profiling and fire plume sampling were deployed to address the deficiencies. The dataset provides a unique opportunity to study the smoke plume structure and plume inject height.

In Deng et al. (2022, hereinafter Part I) we introduced the Wyoming Cloud Lidar (WCL) extinction retrieval and its evaluation with in situ aerosol measurements from a passive cavity aerosol spectrometer probe (PCASP), in situ carbon monoxide (CO) measurements from an Aero-Laser CO instrument, and CO column measurements from the University of Colorado Airborne Solar Occultation Flux (CU AirSOF) instrument. The advantage of the upward-pointing WCL is its ability to gather information on the vertical structure of the smoke plumes at altitudes larger than the aircraft flight level.

The probability density functions (PDFs) and cumulative density function (CDF) of plume top height, optical depth, and plume physical depth of smoke plume layers identified from the WCL measurement during BB-FLUX are shown in Fig. 1. To be clear, the height in this study is height above mean sea level. The occurrence of multiple-layer smoke plumes is 20%, and most of these are double layers. The top heights of these multiple-layer plumes range from 1.5 to 8 km, and their dominant depth is 300 m. In contrast, the occurrence of single-layer plumes is 80%. These have top heights that range from 2 to 6 km and layer depths that range from a few hundred meter to 2.3 km. The single layers have slightly larger optical depth than the multiple layers. This assessment is limited because the WCL only partially sampled in the upward direction, due to attenuation of the WCL's laser, and because attenuation results in underestimation of plume optical depth and physical depth. The North America smoke plumes observed by Raman lidar in Europe (Mattis et al. 2008) had plume top heights from 2 to 8 km and a dominant plume depth of 2 km. In their analysis of measurements from *CALIPSO*, Labonne et al. (2007) showed that plume heights range from 4 to 7 km.

The Figs. 1a–c distributions provide a statistical summary of smoke plumes over the western United States, but they do not connect plume height and depth to horizontal plume extent, plume location relative to the fire source, fire intensity, and the plume environment. Moreover, fire smoke prediction requires observational characterization of smoke plumes and their spatial structure. In Part II, we reconstruct the vertical structure of individual wildfire plume from consecutive WCL transects and determine the smoke plume injection height. Throughout we take advantage of the AirSOF CO column density as an index of fire intensity, along with the in situ measurements of meteorological parameters (humidity, thermal stability, wind, and turbulence), to investigate the possible factors that affect the plume injection height.

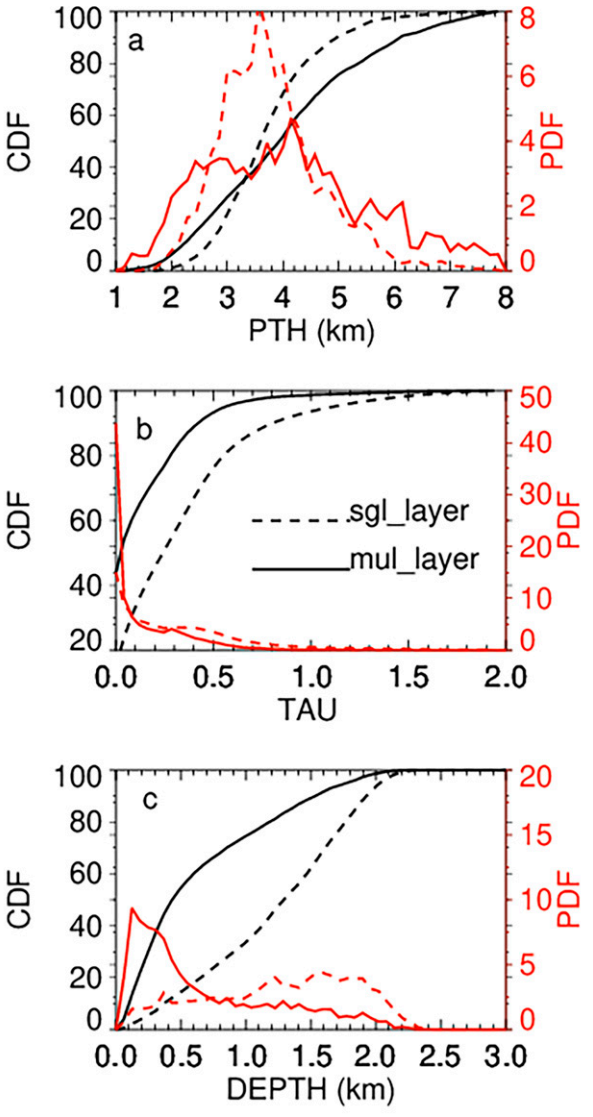

FIG. 1. The cumulative probability function (CDF; black lines) and probability density function (PDF; red lines) of the WCL-identified smoke plume layer top heights (PTH), optical depth (TAU), and layer depth (DEPTH) during the entire BB-FLUX project. Solid lines are for identified multiple layers (100 908 in total) in the WCL profile; dashed lines are for single layers (430 110 in total) in the WCL profiles.

This paper is organized as follows. In section 2, the method used to reconstruct plume vertical cross sections, based on WCL-retrieved aerosol extinctions, is described. In the large context of the WCL cross sections, the in situ measurements are examined in detail to study the plume internal variation. In section 3, seven smoke plumes are investigated using the WCL cross sections and multileg in situ sampling. Section 4 compares the seven plumes in terms of vertical properties of the fire plumes, the plume width, and plume injection heights. The possible factors that affect the plume injection height are explored, such as plume age at a distance downstream of the fire center, CO emission, and meteorological parameters. A final summary is provided in section 5.

2. Reconstruction of fire plume and analysis method

For the BB-FLUX project the flight patterns are designed to include an initial surveillance of the plumes above the fires, and flight legs perpendicular to the mean wind direction to measure the biomass burning fluxes of trace gases and aerosol. Horizontal extensions of flight legs were performed to sample the clear background for remote sensing measurements and ascent/descent profiling was conducted for in situ measurements. During the flight legs perpendicular to the mean wind, the University of Wyoming King Air (UWKA) sampled the fire plume along nearly the same ground track but at different heights to provide a vertical cross section of the fire plume. The lidar was expected to provide a vertically resolved cross section of the fire plume from the lowest flight leg, although the signal was usually attenuated within approximately 200–1000 m in thick plume. Therefore, those flight legs only provided a vertical segment of the plume. To determine the plume injection height from a plume cross section, we reconstructed the vertical structure of the fire plumes using consecutive WCL transects from different flight legs applying the following two steps.

a. *Reconstruction of the vertical and horizontal coordinates according to the flight pattern and wind direction*

The WCL vertical sample resolution is 1.5 m. For the new coordinates, we use 3.0 m as the vertical resolution so that the resulted plume still has high resolution and sufficient WCL sampling. As the horizontal coordinate, either the distance to the plume center or a combination of latitude and longitude coordinates could be used. Because the flight tracks had small deviations between consecutive transects and the location of the plume center could change as the fire evolved, mapping with distance to the plume center could be ambiguous and complicated for the final vertical fire plume reconstruction. The UWKA flew mostly perpendicular to the wind direction while sampling the fire plumes, hence the change of latitude or longitude of the flight track was monotonic. Furthermore, the mapping in latitude or longitude is reliable and suitable for data processing. Therefore, we use latitude or longitude, depending on the wind directions, as the horizontal coordinate with a resolution of 0.004°, which corresponds to about 380 m in distance in the midlatitude. The height and horizontal ranges are selected for each fire plume case according to the UWKA flight patterns.

b. *Mapping of the WCL aerosol extinction coefficients from different flight legs to the reconstructed coordinates*

Where the WCL was fully attenuated, the observation count was set to zero, however, if the WCL-derived extinction coefficient corresponded to smoke or clear sky, the observation was counted. The vertical profile of the mean aerosol extinction coefficient was averaged over the multiple flight legs. Near the plume centerline, the WCL signal tended to be fully attenuated; therefore, the data sample was limited. For the less dense region of the fire plume, the WCL could profile the atmosphere in each transect; therefore, the reconstructed aerosol extinction coefficients would be the averaged fire plume structure over the UWKA sample periods, which ranged from 45 min to 2.5 h. Each flight legs through the fire plumes ranged from 10 to 20 min depending on the plume width.

The reconstructed WCL vertical extinction coefficient cross sections allow one to visualize the vertical structure of the fire plume at a particular time or at a particular downwind distance in a plume evolution. The cross-section structure is related to the time history of fire development and to fire plume transport by wind; therefore, it is an optimal measure for the plume injection heights. It also provides a large context for the understanding and interpretation of in situ measurements at the flight level. Our analysis procedure includes the following steps:

1) Analyze the in situ measurements of aerosol and CO concentration in the context of the reconstructed extinction cross sections.
2) Estimate the vertical profile of plume width and the aerosol concentration-weighted plume width from the reconstructed cross sections. Our assessment of the plume horizontal width is corrected to a Cartesian width using the angle between the flight track and the horizontal coordinate direction, which will be explained in section 4b.
3) Identify the plume injection height from the vertical profiles of plume width. Plume injection height has been defined in several ways in the literature. For example, the plume injection height in satellite measurements is defined as the maximum height in the aerosol feature mask (Raffuse et al. 2012; Kahn et al. 2008; Labonne et al. 2007). The plume flattens as it reaches the injection height (Raffuse et al. 2012); therefore, here it is defined as the height of maximum plume width or aerosol concentration-weighted plume size. The aerosol concentration-weighted plume size appears similar to the technique using weighted aerosol centroid height in Lu et al. (2021).
4) Relate the identified plume injection heights to thermodynamic factors and plume transport.

3. Case studies of vertical fire plume structures

We reconstructed seven fire plumes at different locations, which are noted in red in Fig. 1 in Part I. A complete list of

TABLE 1. Summary list of distance of flight to fire or plume age, temperature T, relative humidity RH, turbulence, wind speed, and fire injection height by fresh plume width in Fig. 10b (by concentration-weighted plume width in Fig. 10d) of the seven fire plume cases. The atmospheric turbulence is evaluated using the cubed root of the eddy dissipation rate ($\varepsilon^{1/3}$; Sharman et al. 2014); T, RH, and turbulence are averaged over the 2–4.5-km height range. Wind speed is averaged over the fire plume range. The warmest, driest, windiest, and most turbulent conditions are highlighted in boldface type. Dates are given as two-digit month and two-digit day (e.g., 0808 = 8 August). Durations are given as hour:minutes.

Date (sample duration), fire name	Distance of flight to fire (km)/age (h)	T (°C)	RH (%)	Turbulence ($m^{2/3}$ s^{-1})	Wind speed (m s^{-1})	PBL top height (km)	Plume injection height by plume width (by weighted plume size) (km)	Mean CO column concentration × 10^{18} molecules cm^{-2}
0808 (1:40), Rabbit Foot	25/1.2	**14.0**	**25**	0.11	6.0	[2.5, 4.5]	3.0 (5.3)	8
0825a (2:30), Watson Creek	30/1.2	6.4	36	0.04	6.5	[1.5, 3.0]	2.8 (2.9)	6
0825b (1:10), Watson Creek	35/1.1	6.9	41	0.06	9.1	[3.0, 4.0]	4.0 (4.0)	12
0831 (2:00), Stewart Creek	25/1.0	6.5	36	**0.13**	7.2	[2.0, 4.0]	3.8 (4.2)	2
0906a (0:45), Miriam	6/0.3	6.5	38	0.06	6.0	[1.5, 3.0]	3.3 (3.3)	2
0906b (1:35), Miriam	10/0.3	6.2	44	0.06	6.7	[3.0, 3.5]	3.2 (3.3)	3
0915 (2:10), Pole Creek	170/2.4	**14.0**	**21**	**0.12**	**15.5**	[3.5, 5.0]	3.5 (5.5)	6

the fire names, distances from the fire centers, meteorological parameters, and plume injection heights are shown in Table 1. We use Python's Geopy library to compute the distance between the fire area and the aircraft's location. The library can estimate the geodesic distance between two given points. We calculated the mean geodesic distance using the fire center coordinates taken from the incident report system (InciWeb) and the aircraft position coordinates taken when the plane sampled the fires. The plume age was estimated using the distance divided by the averaged wind speed measured on the aircraft.

a. Double-smoke layer in Rabbit Foot fire on 8 August

The Rabbit Foot fire at the border of Idaho and Montana took place on 8 August 2018. The UWKA sampled eight legs of the fire plume at about 25 km downstream (age of 1.2 h) of the fire center (Table 1) at different height levels from 1.5 to 5 km (Fig. 2a).

The height, longitude, and latitude of UWKA tracks are shown in Figs. 2a–c. The UWKA flight track shows a clear zigzag latitude pattern with time. According to the flight pattern, we constructed the new coordinate with a vertical range from 1 to 6 km and a horizontal coordinate range from 44.5° to 45°N. The CO column density measured from CU AirSOF (Fig. 2d) at 1.5-km flight height was about 8×10^{18} molecules per cm^2. The WCL-derived CO column shows a very similar temporal variation in the enhancements when passing underneath the plume, but it is smaller than the CU AirSOF measurements and maximizes at approximately 4×10^{18} molecules per cm^2. This difference is due to attenuation of the WCL signal.

The eight WCL flight cross sections mapped to the new coordinates are shown in Fig. 2h and show a double-layer structure of the smoke plume. The fire plume below 4 km was embedded in the boundary layer aerosol, which was centered at the about 44.7°N with maximum extinction coefficient at about 1 km^{-1} with little vertical variation, indicating a well-mixed layer. The fresh fire plume above 3 km was tilted to the north, and its top reached about 5.5 km with an extinction coefficient of about 5 km^{-1}. The in situ aerosol concentrations from PCASP measurements (Fig. 2e) and WCL extinction coefficients (Fig. 2f) at the different flight level had a very good correlation with each other, as shown in the statistical analysis in Part I. They also consistently change with the vertical intensification and the horizontal shift in Fig. 2h. Below 3 km (black and blue lines in Figs. 2e,f), they were flat on the southern part of the plume, indicating a well-mixed background layer, but the northern side decreased gradually to the southern level. The background aerosol concentration and optical depth at the sides of the fire plume were about 1000 per cm^3 and 0.2, respectively. In the dense fire plume top above 3 km (green, orange, and red lines in Figs. 2e,f), the aerosol concentration reached about 20 000 per cm^3, which is about 20 times the background aerosol concentration.

The reconstructed extinction coefficient cross section in Fig. 2h shows three vertical segments in the fresh plume center because the ascending/descending WCL transects were attenuated within 0.2–1 km. The optical depths of WCL transects in Fig. 2g are generally smaller than 2. However, the composite optical depth (thick dashed line in Fig. 2g) calculated from the reconstructed extinction coefficients in Fig. 2h maximizes at 4.5 at the fresh plume center. Since the WCL can only observe three vertical segments of the fresh plume center, we can speculate that its total optical depth should be larger than 5.

b. Strong diurnal variation in Watson Creek fire on 25 August

The Watson Creek fire in south-central Oregon was sampled on 25 August 2018. Its plume was sampled for 2.5 h in the morning at about 30 km (about 1.3 h) downstream of the fire center from 1.5 to 5 km (Fig. 3a). The CO column density from CU AirSOF maximized about 7×10^{18} molecules per cm^2. The WCL-derived CO again showed a similar temporal variation but smaller enhancements relative to CU AirSOF measurements.

The reconstructed extinction cross section (Fig. 3h) shows that the fire plume was confined below 3.8 km with very high

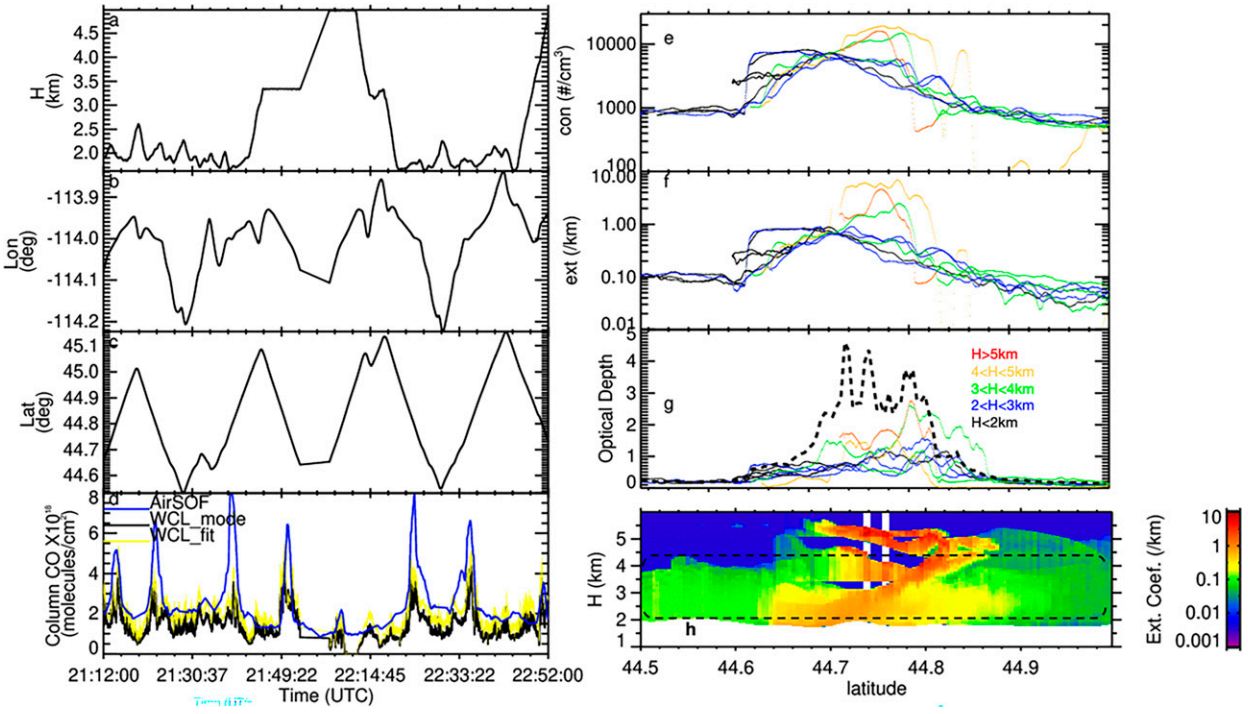

FIG. 2. For the Rabbit Foot fire on 8 Aug 2018, time series of (a) UWKA flight height, (b) latitude, (c) longitude, (d) column CO concentration from AirSOF measurements (blue line) and derived from the WCL using the PDF mode (black line) and fit method (yellow line), which were described in Part I. Also shown are data from consecutive flight legs of (e) in situ aerosol concentrations from the PCASP, (f) WCL-retrieved aerosol extinction coefficients averaged within 150 m of the UWKA flight level, and (g) WCL-measured aerosol optical depth. They are color-coded for measurements at different flight height levels: below 2 km is black, between 2 and 3 km is blue, between 3 and 4 km is green, between 4 and 5 km is orange, and above 5 km is red. The composite mean optical depth from the reconstructed extinction coefficient in (h) is plotted in (g) as a thick dashed line. (h) Composite plume vertical extinction coefficients of the Rabbit Foot fire on 8 Aug 2018; its PBL heights examined from the UWKA wind, potential temperature, and humidity profiles during the sampling period are denoted with dashed lines.

extinction coefficients in the fire plume center and in the boundary layer. The WCL signals at the fire plume center could only reach to about 3 km, while the observed edges of the fire plume extended to 4 km. The fire plume seemed embedded in a denser boundary layer aerosol layer relative to the Rabbit Foot fire in section 3a. The in situ aerosol concentration and extinction coefficients at flight level had less obvious vertical variations than the Rabbit Foot fire. The aerosol concentration and optical depth on the southern side of the fire plume were flat at about 2000 per cm^3 and 0.5, respectively. In the dense fire plume, the aerosol concentration and the composite optical depth reached about 20 000 per cm^3 and 5, respectively, which were more than 10 times as large as the background aerosol.

The UWKA sampled the Watson Creek fire for a second time one hour later in the afternoon with stacked flight heights from 1.5 to 5.5 km at about 35 km (~1.1 h) downstream of the fire center. The CO column concentration from CU AirSOF (Fig. 4d) maximized about 16×10^{18} molecules per cm^2, which was about 2.5 times that in the morning. It had the most intensive CO emission among the seven cases. The extinction coefficient cross section in Fig. 4h shows a more complete fresh plume cross section than the Rabbit Foot fire plume. The extinction coefficients decrease from the center to both side edges. The plume horizontal width increases linearly with height. This finding is consistent with the plume cross sections observed with scanning Doppler lidar in Lareau and Clements (2017), indicating the strong uplift of aerosol or plume rise. However, in Fig. 4h, the extinction coefficient increases with height, which is opposite to the finding in Lareau and Clements (2017).

The fire plume top was around 4.5 km, which was taller than the morning fire plume. The aerosol on the side of the plume had aerosol number concentration of 1000 per cm^3 and optical depth of 0.1, which was reduced by a factor of 2, relative to the morning plume. The fire plume top at 4.5 km included pockets of aerosol with number concentrations reaching up to 30 000 per cm^3 and extinction coefficients up to 10 km^{-1}. The composite optical depth at the fire plume center shown in Fig. 4g was 10. The comparison of the in situ and remote sensing measurements as well as the extinction cross section in the morning and the afternoon suggests that the Watson Creek fire plume intensified in the afternoon, while the boundary layer aerosol concentration decreased.

c. *Weak smoke plume in Stewart Creek fire on 31 August*

The Stewart Creek fire occurred in central of Idaho. On 31 August 2018, the UWKA sampled the fire plume for about

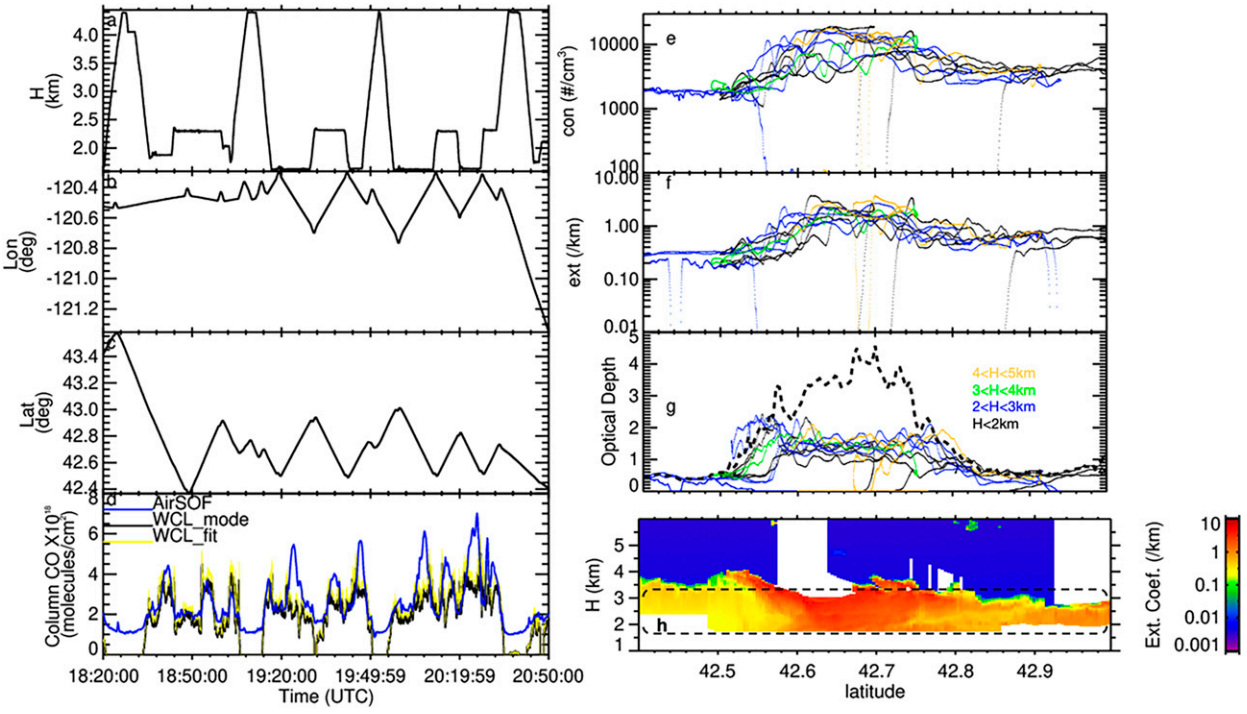

FIG. 3. As in Fig. 2, but for the Watson Creek fire in the morning on 25 Aug 2018.

2 h at about 25 km (~1.1 h) downstream. The CO columns from CU AirSOF (Fig. 5d) peaks around 2×10^{18} molecules per cm^2. For the smoky peaks, the CO columns from the CU AirSOF and WCL derivation are close to each other, but for the background aerosol region, the AirSOF is generally larger than the WCL derivation. There are two possible reasons for this. First, the correlation of the WCL extinction and NCAR CO concentration in Fig. 8 in Part I in the small extinction

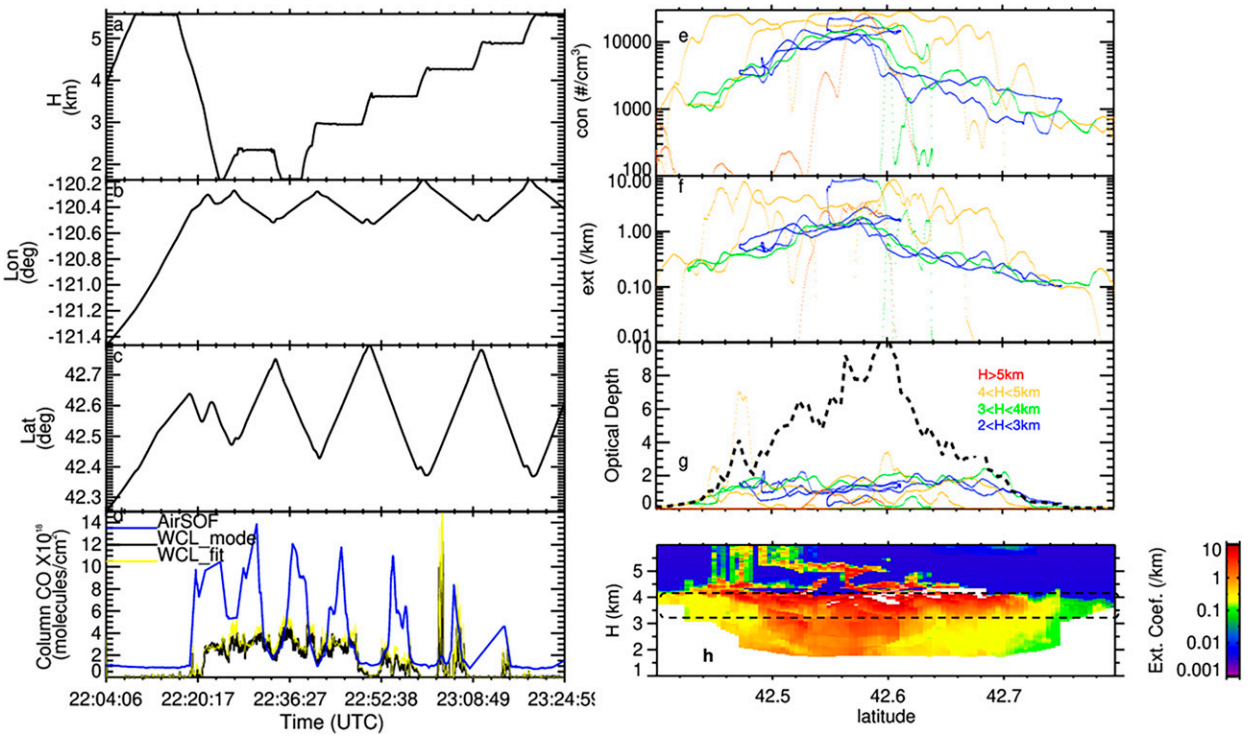

FIG. 4. As in Fig. 2, but for the Watson Creek fire in the afternoon on 25 Aug 2018.

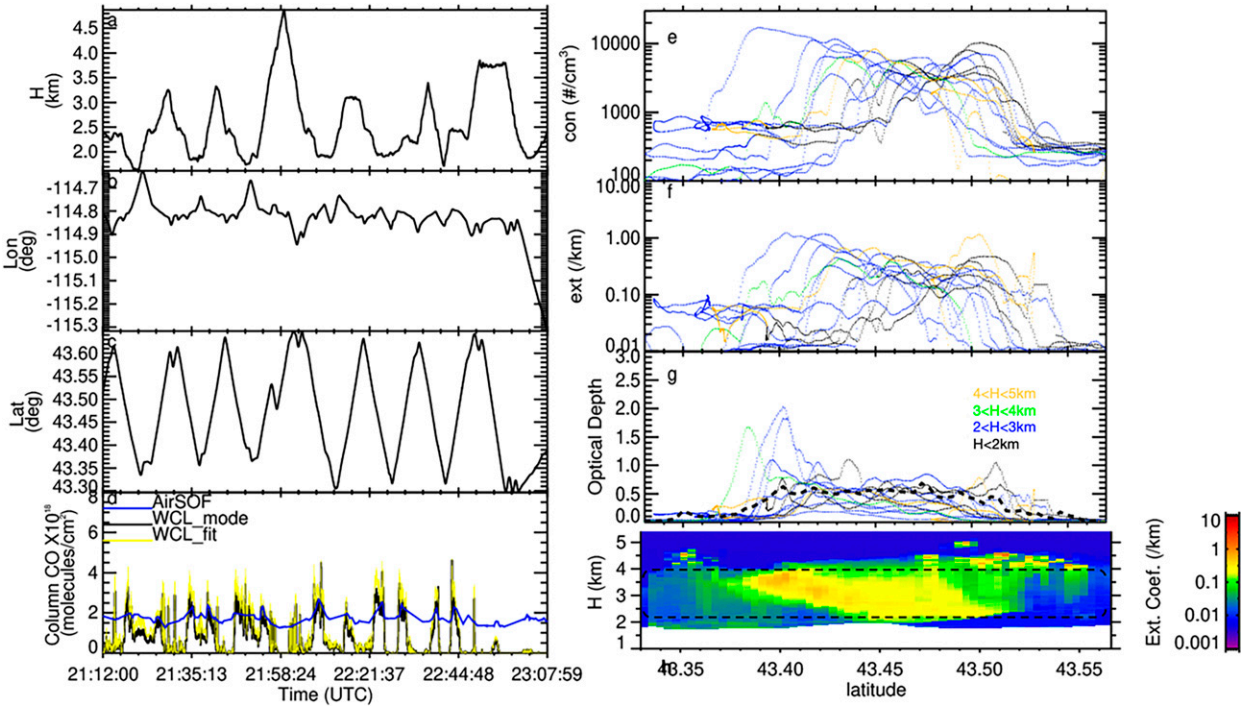

FIG. 5. As in Fig. 2, but for the Steward Creek fire on 31 Aug 2018.

coefficient region is poorer; therefore, the WCL-derived CO column has a larger error. Second, we can see that the AirSOF CO column concentrations in Figs. 2d, 3d, and 4d are seen to minimize at about 1×10^{18} molecules per cm^2, which might be the minimum sensitivity of the AirSOF measurement.

The extinction coefficient cross section in Fig. 5h is showing a fire plume that seems lofted above 2 km since there was a minimum extinction coefficient around the smoke plume base. The plume was confined below 4.5 km with a left-side skewed vertical structure where extinction coefficients were generally less than 1 km^{-1}. The background environment on the sides was relatively clearer than the previous cases with aerosol concentrations measured from PCASP (Fig. 5e) of less than 500 per cm^3, and aerosol optical depth (Fig. 5g) of about 0.1. The in situ aerosol concentration and extinction coefficients at flight levels had small vertical variations and the vertical tilting. The composite optical depth of the fire plume was around 0.5, which was smaller than some of WCL transects, especially on the southern side, indicating that the reconstructed WCL aerosol extinction coefficients was the averaged WCL observations over the 2-h periods and the southern edge of the fire plume had larger temporal and spatial variations. Even for a weak smoke plume like Stewart Creek fire, the active fire plume top tended to have denser aerosol.

d. Weak diurnal variation in Miriam fire on 6 September

The Miriam fire occurred in south-central of Washington State. On 6 September 2018, the UWKA sampled it for less than 1 h in the morning at about 6 km (about 15 min) downstream of the fire center, which was sampled closest to the fire source. The column CO concentrations from CU AirSOF (Fig. 6d) maximized around 2×10^{18} molecules per cm^2, which is the smallest value for the seven cases. The WCL measurements agreed with the CU SOF measurements. The extinction cross section in Fig. 6h shows that a small fire plume was embedded in a relatively dense layer of background aerosol below 3 km, which was confirmed by the in situ aerosol concentration in Fig. 6e at 2000 per cm^3. The center of the plume shot up to 4 km, thick aerosol detrained from the center to the western side at about 3 km like anvil clouds. The in situ aerosol concentrations and flight level extinction coefficients in the fire plume in Figs. 6e and 6f increased very little with height. The composite optical depth maximizes at 1, which is similar to the individual WCL transect.

About 75 min later, the UWKA sampled the Miriam fire for about 1.5 h in the afternoon. The column density of CO from CU AirSOF measurements maximized at 3×10^{18} molecules per cm^2. The WCL-derived CO concentration agreed very well with CU SOF measurements except for the finer temporal structures. The reconstructed WCL extinction coefficient cross section is shown in Fig. 7h. When compared with the morning measurements, the background aerosol seemed to be diluted a little since the in situ concentrations and the flight level extinction coefficients decreased by a factor of 2. The fire plume spread slightly more horizontally in the afternoon. In comparison with the Watson Creek fire, this fire did not seem to intensify as strongly in the afternoon.

e. Double-layer smoke in Pole Creek fire on 15 September

The Pole Creek fire occurred at the northeast corner of Utah. On 15 September 2018, the fire smoke was transported

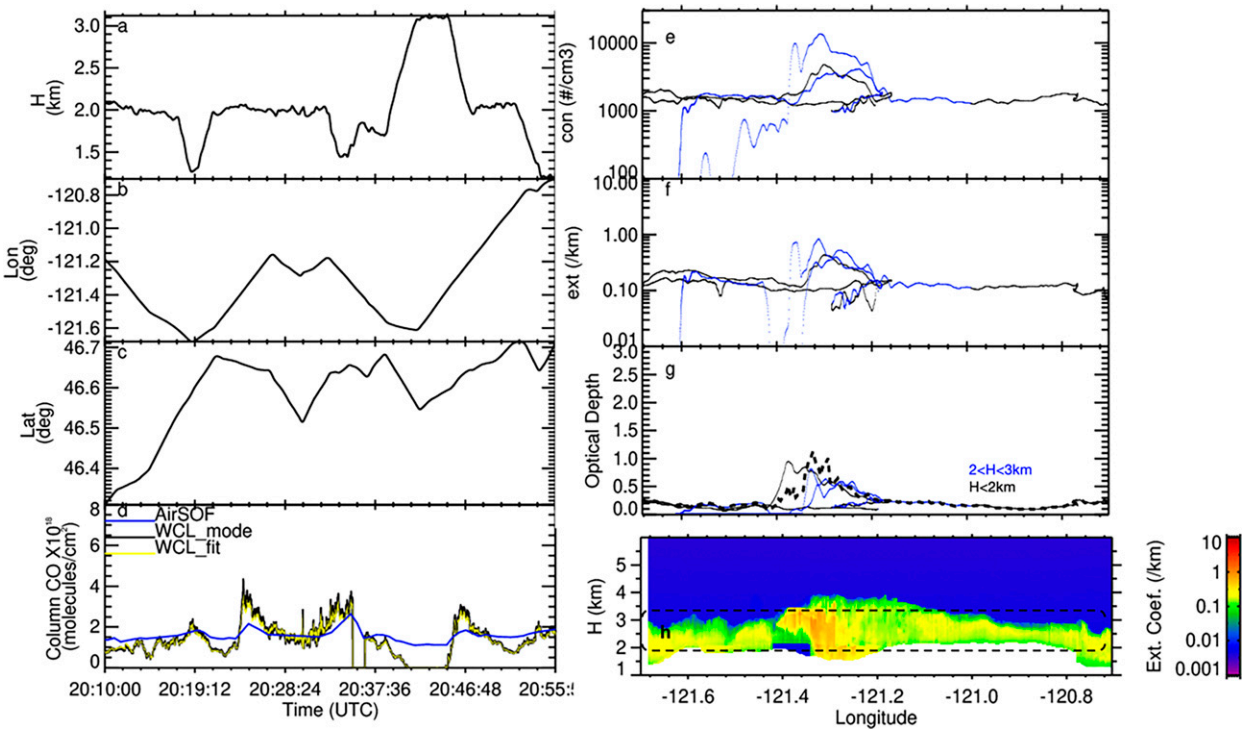

FIG. 6. As in Fig. 2, but for the Mariam fire in the morning on 6 Sep 2018.

northeasterly quickly due to the strong wind. The UWKA sampled it for more than 2 h in the afternoon at about 170 km (~2.4 h) downstream of the fire center. For the seven cases analyzed, the distance is the largest. The UWKA sampled the fire from 2 to 6 km since the fire had the highest fire plume top. The extinction cross section in Fig. 8h, shows a similar double-layer vertical structure as the Rabbit Foot fire on 8 August (Fig. 2h). The fire plume below 3.5 km seemed well mixed with little vertical variation. The extinction coefficients and aerosol concentrations decreased from the fire plume center at about 1.0 km^{-1} and 10 000 per cm^3 to less than 0.01 km^{-1} and less than 500 per cm^3 in the background, respectively, indicating a cleaner environment in the Salt Lake City (Utah) Valley. Above 3 km, the UWKA flew through the fire plume with three trapezoid transects. The WCL signal was fully attenuated in 500 m in the fire plume center, leaving a big gap in the vertical structure in Fig. 8h. Wavelike structures are evident on the eastern side of this smoke plume at 5–6 km. The crosswind spreading at 5–6 km is farther than the lower boundary layer spreading.

4. Intracomparison of the fire plume cases

a. *Vertical properties of the fire plumes from in situ and WCL measurements*

The mean vertical profiles of the fire plume properties from in situ measurement during the plume sample period are shown Figs. 9a–c. The mean WCL-derived aerosol concentration and depolarization ratio from the reconstructed cross section are shown in Figs. 9d and 9e. The in situ measured CO concentration and PCASP aerosol number concentration are positively correlated in Figs. 9a and 9b. These CO and aerosol values are largest in the Watson Creek (0825; blue line), and the top layers of Pole Creek (0915; orange line) and Rabbit Foot (0808; black line) plumes, especially at the fire plume top. The CO concentration of Watson Creek fire in the morning was around 800 ppbv, whereas it almost doubled in the afternoon as the plume top increased from 3.5 to 4.5 km. The CO values for the Stewart Creek fire (0831; green) and Mariam fire (0906, red lines) were less than 300 ppbv overall.

Applying the mean relationships between PCASP aerosol concentrations and the WCL extinction coefficients (Fig. 8 and Table 1 in Part I), we generated the aerosol concentration vertical cross sections from the extinction cross sections. The resulted mean vertical profile is shown in Fig. 9d. Relative to the in situ measurement, the WCL-derived concentrations extend the in situ data for a much clearer vertical pattern beyond the flight altitudes. The WCL-derived aerosol concentrations within the Pole Creek (Orange), Rabbit Foot (black), and Watson Creek (blue) plumes increased with height to the plume top with lots of fine fluctuations as the in situ measurements did in Fig. 8b, whereas the WCL derivation extended the in situ data for a much clearer vertical pattern beyond the flight altitude. This fine fluctuation is consistent with the vertical structures in Figs. 2, 4, and 8, and indicate that the tops of these of strong active fire plumes hold pockets of the large CO and aerosol concentrations. Lareau and Clements (2017) examined one plume vertical cross section using Doppler lidar measurement. They also found smoke backscattering fluctuations, which is correlated with

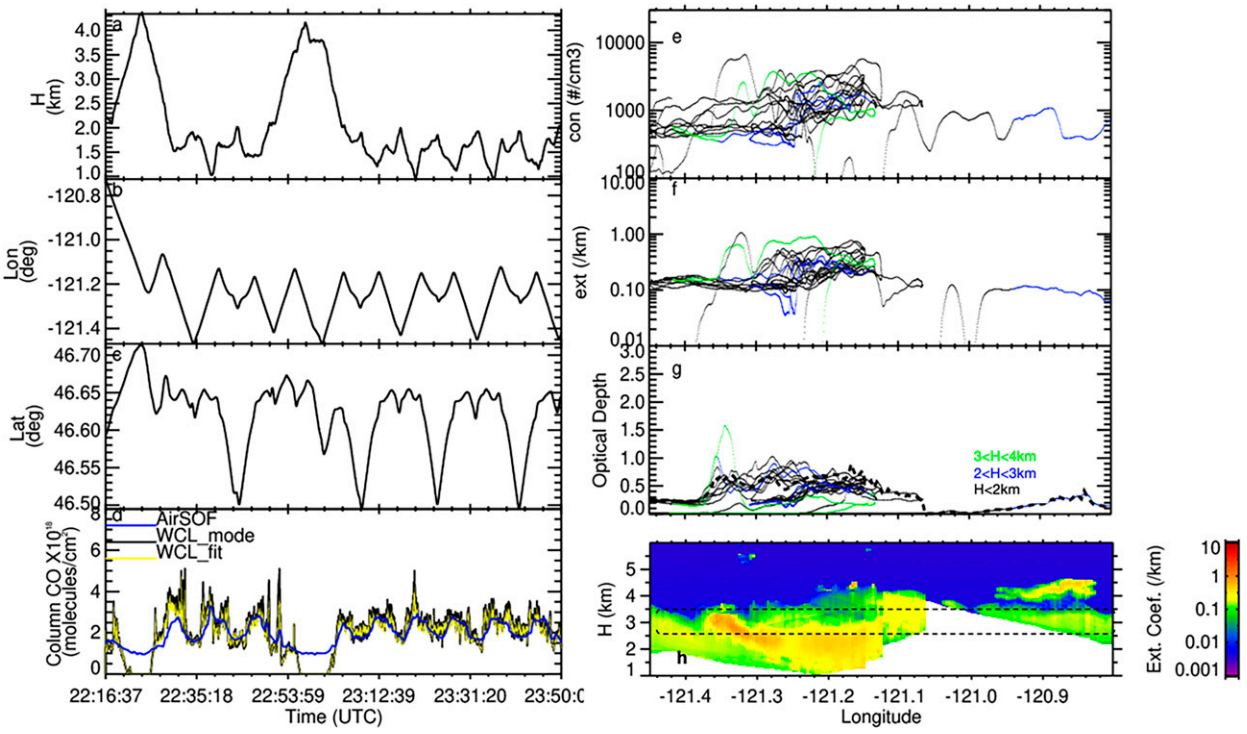

FIG. 7. As in Fig. 2, but for the Mariam fire in the afternoon on 6 Sep 2018.

radial velocity fluctuation. The coherent smoke–velocity fluctuations redistribute smoke outward from the plume core and mix clear air inward. In the case of the Pole Creek fire, these CO and aerosol enhanced concentrations were associated with maximal values of depolarization (Fig. 9e) suggest the presence of nonspherical aerosol particles. In the two Miriam cases, the depolarization values increased in the downward direction and maximized at 1.8 km.

The mean vertical profiles of the PCASP-derived aerosol mass mean diameters D_{mm} are shown in Fig. 9c. The D_{mm} of the Watson Creek fire, in the afternoon, and the Pole Creek fire increased with increasing height and reached up to more than 0.25 μm at the plume top, consistent with the WCL-measured linear depolarization ratio (LDR) profiles in Fig. 9e, although the LDR of the Pole Creek fire was overall larger than in the other cases, probably indicating more large irregular aerosol particles were being pumped into the upper troposphere. The D_{mm} in plume in the Watson Creek fire, in the morning, and the Miriam Creek fire decreased slightly with increasing height, as did their LDRs, shown in Fig. 9e.

b. *Vertical distributions and plume injection heights from WCL measurements*

The vertical profiles of plume widths, derived from the extinction cross sections in Figs. 2–8, are shown in Figs. 10a–d. The plume widths in the four panels are calculated by first counting all aerosol occurrence (Fig. 10a), thick fire plume occurrence after excluding the background aerosol with an extinction coefficient threshold of 0.2 km^{-1} (Fig. 10b), concentration-weighted all aerosol occurrences (Fig. 10c), and concentration-weighted thick fire plume occurrence at each height level (Fig. 10d). These counted plume widths are then corrected using the angle between the flight track and the mapping horizontal coordinate. The actual plume widths are normalized by the maximum width of the Pole Creek fire for a relative size comparison in Fig. 10.

The ranks of the plume width corresponding to all aerosols (Fig. 10a) were Pole Creek (0915; orange), Miriam morning (0906a; solid red), Watson Creek morning (0825a; solid blue), Miriam afternoon (0906b; dashed red), Rabbit Foot (0808; black), Watson Creek afternoon (0825b; dashed blue), and Stewart Creek fires (0831; green). However, the amplitude of these vertical profiles is somewhat diminished in the Rabbit Foot and Pole Creek cases because of WCL attenuation. In addition, the ambient aerosol abundance was stronger in the Miriam morning case than in the others.

The ranks of the plume width of fresh thick plume (Fig. 10b) were Pole Creek (0915; orange), Watson Creek morning (0825a; solid blue), Watson Creek afternoon (0825b; dashed blue), Miriam afternoon (0906b; dashed red), Miriam morning (0906a; solid red), Rabbit Foot (black), and Stewart Creek fires (green). As compared with findings discussed in the previous paragraph, the Miriam morning/afternoon pair ranked in reverse. This is because of the exclusion of the ambient aerosol from the Miriam morning case. Also, Watson Creek afternoon fire ranking increased because of afternoon intensification of that fire noted earlier. The height of their maximum plume width of the thick fire plumes (as the plume injection height) were 3.5 km (0915; orange), 2.8 km (0825a; solid blue), 4.0 km (0825b; dashed blue), 3.2 km (0906b;

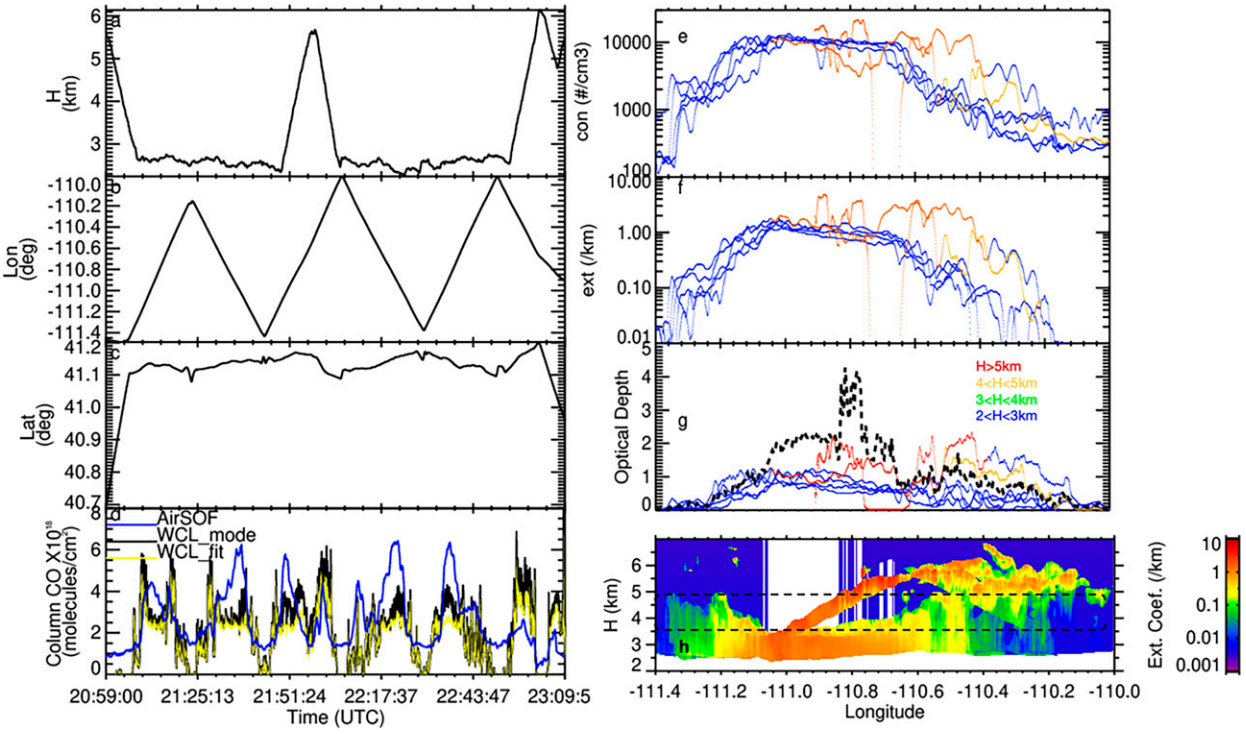

FIG. 8. As in Fig. 2, but for the Pole Creek fire on 15 Sep 2018.

dashed red), 3.3 km (0906a; solid red), 3.0 km (0808; black), and 3.8 km (0831; green), which are all below 4 km.

The aerosol concentration-weighted plume width, shown in Figs. 10c and 10d, made the top layers of the Rabbit Foot and Pole Creek fires, and the Watson Creek afternoon fire more prominent because of the aerosol concentration vertical stratification. Their weighted plume widths quickly decrease with height above their peaks at 5.3, 5.5, and 4.0 km, respectively. In these cases, the plume injection height defined by aerosol concentration-weighted plume size and the slope of aerosol concentration should be consistent. The plume injection heights from the fresh plume width in Fig. 10b and the concentration-weighted fresh plume width Fig. 10d peaked at one of the double aerosol layers of the Rabbit Foot and Pole

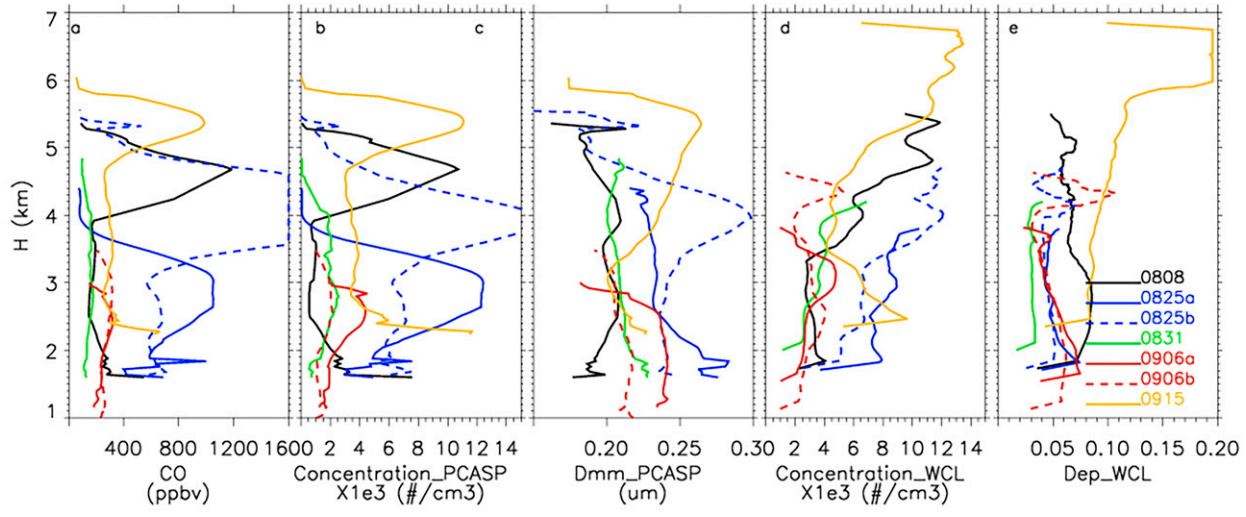

FIG. 9. Mean vertical profiles of (a) in situ sampled CO concentration, (b) PSCAP aerosol number concentration (number per cm^3, scaled by 10^{-3}), (c) PCASP-derived mass mean diameter averaged during the plume sampling period, (d) WCL-derived aerosol concentration, and (e) WCL depolarization ratio averaged over the thick plume in the reconstructed cross sections in Figs. 2h–8h.

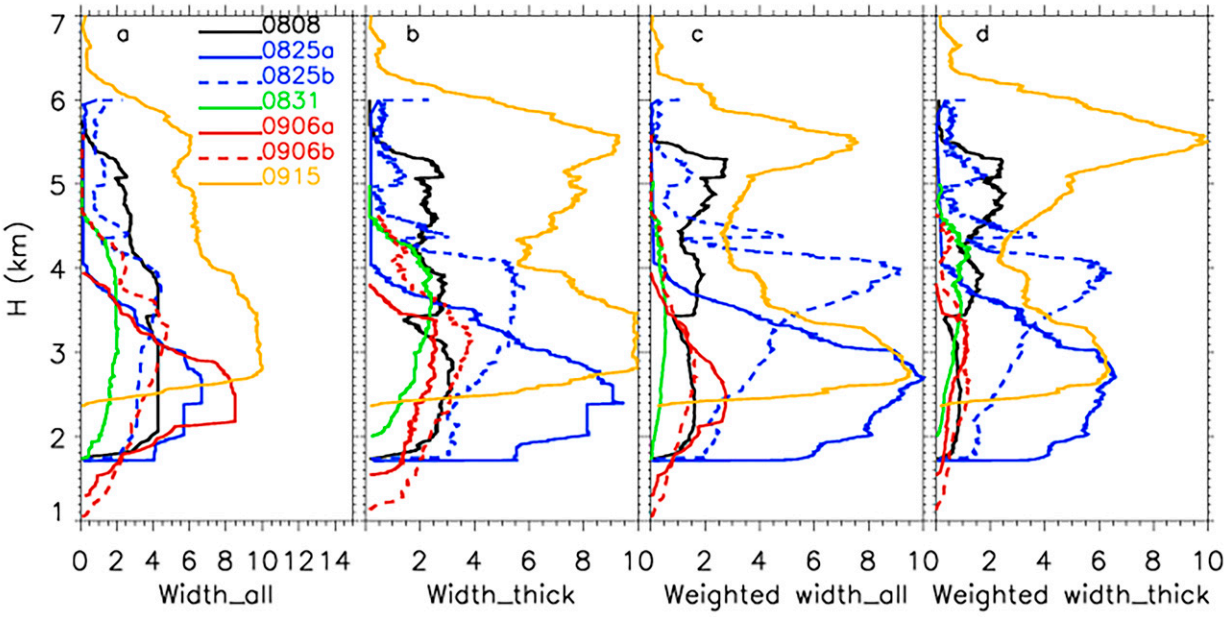

FIG. 10. Vertical profiles of relative plume width from (a) all aerosol, (b) thick fire plume, (c) concentration-weighted all aerosol, and (d) concentration-weighted thick fire plume. They are all normalized by the maximum width of the Pole Creek fire.

Creek fire. However, the plume injection heights from two calculation methods were very similar in the Watson Creek, Steward Creek, and Miriam fires.

The plume sizes calculated from the four methods show different characteristics about the plume. The resulted plume injection height depends on whether the instrument can discriminate the background aerosol and the fresh plume, and whether it is defined by smoke size or smoke aerosol concentration-weighted plume size.

c. *Vertical thermodynamic structures and PBL heights*

The injection height of a smoke plume is controlled by the plume dynamics, which are driven by both the energy released by the fire and the ambient atmospheric conditions (Kahn et al. 2007; Labonne et al. 2007). For example, the ambient atmospheric stability acts on the level of plume uplifting, and the degree of turbulent mixing occurring at the edge of the plume affects the entrainment and detrainment of ambient air into the plume, decreasing positive plume buoyancy, and decreasing the vertical transport of smoke to the free troposphere (Kahn et al. 2007).

Figure 11 shows the time-mean vertical profiles of the meteorological parameters from the UWKA. Below 4 km, the temperature profiles of Rabbit Foot (0808; black) and Pole Creek (0915; orange) fires in Fig. 11a were about 10°C warmer than other cases. The relative humidity below 4 km in Fig. 11c shows that the Pole Creek fire was the driest, seconded by the Rabbit Foot fire, which were 10%–20% drier

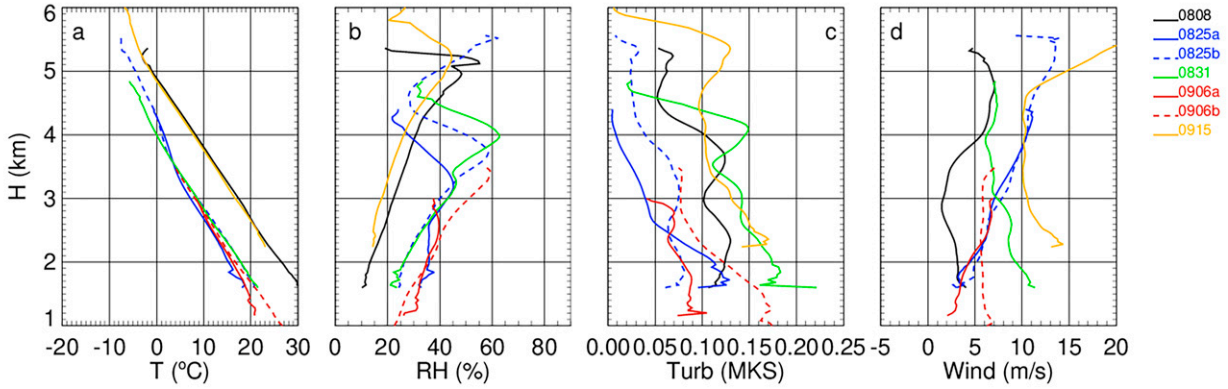

FIG. 11. Time-mean vertical profiles of (a) temperature, (b) relative humidity, (c) turbulence, and (d) wind speed from the UWKA aircraft measurements during the plume sampling period.

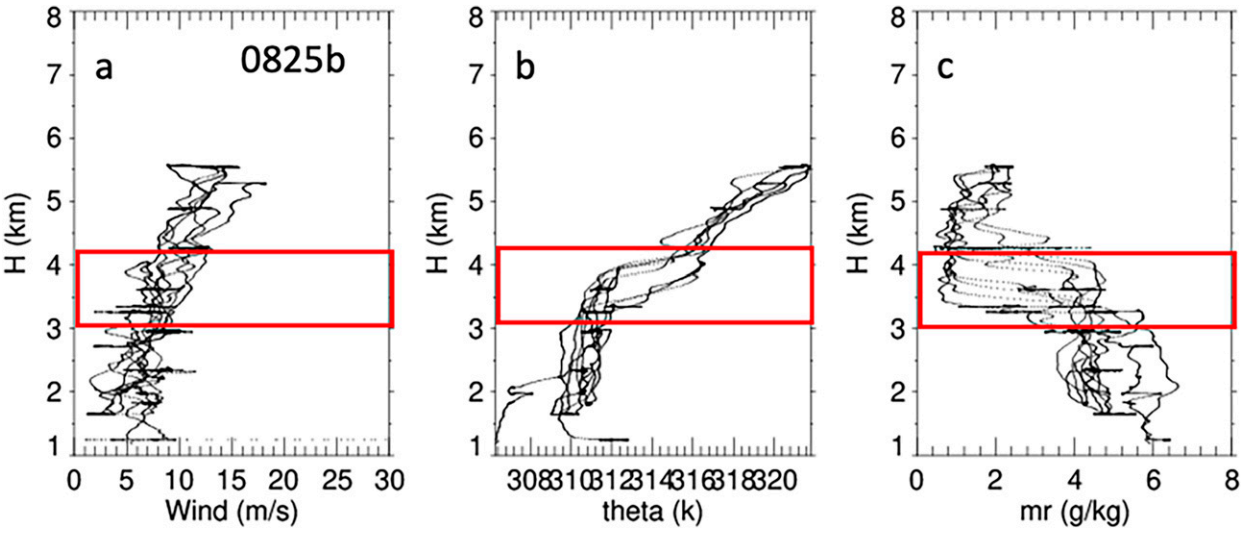

FIG. 12. The UWKA instant profiles of wind speed, potential temperature (theta), and water vapor mixing ratio for the 0825b plume sampling in Fig. 5. The estimated boundary layer top height is highlighted in the red-outlined boxes.

than other cases. The turbulence or eddy dissipation rate in both the Pole Creek and Rabbit Foot fires were also strong. The wind speed in Pole Creek fire was the highest, while the Rabbit Foot had the lowest wind speed of all cases, which supports that the Pole Creek plume size was much larger than the Rabbit Foot fire.

To relate the plume injection height with the PBL height, we estimated the PBL height from the UWKA instant profiles of wind speed, potential temperature, and water vapor mixing ratio. One example is shown in Fig. 12 for Watson Creek fire plume in the afternoon. Relative to the free troposphere, the boundary layer is associated with lower wind speed and/or higher water vapor mixing ratio. The top of the PBL is often associated with a steep increase of potential temperature with height. For the case in Fig. 12, the PBL top is from 3 to 4 km where increases of potential temperature and decreases of water vapor mixing ratio are evident. The wind speed has no obvious change in this region for this case. A similar method for PBL top determination was applied in Lareau and Clements (2017). The PBL top heights for the seven cases are listed in Table 1 and shown in Figs. 2h, 3h, 4h, 5h, 6h, 7h, and 8h within dashed black lines. Except for the Rabbit Foot (0808) and Pole Creek (0915) cases, 90% of the fire smoke is within the PBL. For the Rabbit Foot and Pole Creek fires, the PBL top heights reach 4.5 and 5 km, respectively, which are higher than other cases. The plume inject heights for these two cases by fresh plum width are 3.0 and 3.5 km (Fig. 10b) and are below the PBL top heights. However, their second smoke layers penetrated through the PBL and brought up the very dense smoke aerosol. For the Pole Creek case, this higher layer was spread even farther than the boundary layer shown in Fig. 8h. This finding may indicate that the buoyant smoke plume layer that breaks through PBL tends to be transported farther downwind (Wandinger et al. 2002; Müller et al. 2005; Mattis et al. 2008; Baars et al. 2021).

The plume injection height varies as the plume transports. We are aware that WCL cross section is just one slice of the plume at a particular distance and age. The Miriam fire plumes on 0906 were about 15 min away from their fire center, and it had a relatively small plume width among the seven cases. Pole Creek fire on 0915 was observed at the largest downwind distance and had the tallest and broadest plume. The Rabbit Foot (0808), Watson Creek (0825), and Steward Creek fire (0831) were sampled around 1 h away from their fire centers. Watson Creek fire plumes were wider than the Stewart Creek plume, and the Rabbit Foot fire plume was taller than the Steward Creek fire plume, indicating that plume size and height also depend on the fire development. The fire CO mass flux can be calculated by integrating the product of vertical column density and wind fields normal to the flight for the smoke plume underpass. The fire duration, burned area, CO mass fluxes, and FRP of these fire cases are examined in Romero-Alvarez et al. (2022, manuscript submitted to *ACS Earth Space Chem.*). Mass fluxes, burned area, and FRP in the Pole Creek, Rabbit Foot, and Watson fires were much larger than those in the Steward Creek and Mariam fires.

5. Summary

As the Part II of the wildfire smoke observation in western United States from airborne WCL measurement during the BB-FLUX Project, the vertical structures of fire plumes were reconstructed with consecutive WCL transects for seven cases from five different wildfires, which were sampled by UWKA at different distances from their fire centers, ranging from 6 to 170 km. Plume age was between 0.3 and 2.4 h. The vertical structures of the fire plume cross sections and in situ measurements at different heights showed the fire plumes exhibited different macrophysical and microphysical properties. The main points that we found from this study are as follows:

1) The seven cases had a plume injection height between 2.8 and 4.0 km. Most aerosol within this layer were well mixed, and most were confined within the boundary layer. For fire plumes that penetrated through the boundary layer top, such as the Rabbit Foot and Pole Creek fires, they formed a lofted plume layer at around 5.5 km. This plume layer reached the free troposphere and then could be transported over very long distances.
2) UWKA sampling was conducted at a distance from the fire center, which was variable in plume evolution/transport. The Pole Creek fire plume was sampled at the largest downwind distance and was largest in both the vertical and crosswind directions. It exhibited aerosol above the boundary layer top. The Miriam fire plumes on 0906 were about 15 min away from their fire center, and they had the relatively small plume width among the seven cases. This observation is consistent with the notion that injection into the free troposphere can occur in association with plume transport.
3) Plume diurnal variation depends on the fire emission and the PBL height. The comparison of the Watson Creek fire in the morning and in the afternoon showed that the plume of this active strong fire was uplifted in the afternoon as the PBL height increased. However, the Miriam fire plume did not change a lot in the afternoon, and a very little thermodynamical change in the PBL was found in that case.
4) The plume structure was relatable to the thermodynamic characteristics of the PBL and fire intensity. The mass fluxes, burned area, and FRP in Pole Creek, Rabbit Foot, and Watson fires were much larger than those in the Steward Creek and Mariam fires; therefore, the plume size is smaller, and the plume height is lower in Steward Creek and Mariam fires. The highest elevated plumes in the Rabbit Foot and Pole Creek fires had the warmest and driest boundary layer. Additionally, the Pole Creek fire had the highest wind speed and turbulence kinetic energy. These ambient properties likely enhanced the crosswind and vertical spreading of the Pole Creek fire.
5) The WCL-based aerosol concentration and depolarization data showed that nonspherical particles and enhanced aerosol particle concentrations coexisted at the top of Pole Creek plume top. In a less-active fire (Miriam), the degree of depolarization increased somewhat in the downward direction and maximized rather low in the plume. Since the depolarization signal is indicative of the presence of nonspherical aerosol particles, future studies of the aerosol interactions in fire plumes may benefit from the depolarization capability of the WCL and other lidars.

The WCL processing technique described in this study demonstrated that the flight pattern design is important for plume sampling. During BB-FLUX, only an upward WCL was deployed. In the future, a combination of upward- and downward-pointing lidars and along-plume sampling will be proposed to enhance understanding of the plume transport and aging processes.

Acknowledgments. We thank the University of Wyoming King Air team for the successful deployment of the project. The 2018 BB-FLUX campaign is supported under U.S. National Science Foundation (NSF) Award AGS-1754019 (PI: Rainer Volkamer). The WCL data analysis is supported by University of Wyoming King Air corporative agreement funded by NSF.

REFERENCES

Baars, H., and Coauthors, 2021: Californian wildfire smoke over Europe: A first example of the aerosol observing capabilities of Aeolus compared to ground-based lidar. *Geophys. Res. Lett.*, **48**, e2020GL092194, https://doi.org/10.1029/2020GL092194.

Damoah, R., and Coauthors, 2004: Around the world in 17 days—Hemispheric-scale transport of forest fire smoke from Russia in May 2003. *Atmos. Chem. Phys.*, **4**, 1311–1321, https://doi.org/10.5194/acp-4-1311-2004.

Deng, M., and Coauthors, 2022: Wildfire smoke observations in the western United States from the airborne Wyoming Cloud Lidar during the BB-FLUX project. Part I: Data description and methodology. *J. Atmos. Oceanic Technol.*, **39**, 545–558, https://doi.org/10.1175/JTECH-D-21-0092.1.

Derwent, R., D. Stevenson, W. Collins, and C. Johnson, 2004: Intercontinental transport and the origins of the ozone observed at surface sites in Europe. *Atmos. Environ.*, **38**, 1891–1901, https://doi.org/10.1016/j.atmosenv.2004.01.008.

Duck, T. J., and Coauthors, 2007: Transport of forest fire emissions from Alaska and the Yukon Territory to Nova Scotia during summer 2004. *J. Geophys. Res.*, **112**, D10S44, https://doi.org/10.1029/2006JD007716.

Griffin, D., and Coauthors, 2020: The 2018 fire season in North America as seen by TROPOMI: Aerosol layer height intercomparisons and evaluation of model-derived plume heights. *Atmos. Meas. Tech.*, **13**, 1427–1445, https://doi.org/10.5194/amt-13-1427-2020.

Kahn, R. A., W.-H. Li, C. Moroney, D. J. Diner, J. V. Martonchik, and E. Fishbein, 2007: Aerosol source plume physical characteristics from space-based multiangle imaging. *J. Geophys. Res.*, **112**, D11205, https://doi.org/10.1029/2006JD007647.

——, Y. Chen, D. L. Nelson, F.-Y. Leung, Q. Li, D. J. Diner, and J. A. Logan, 2008: Wildfire smoke injection heights: Two perspectives from space. *Geophys. Res. Lett.*, **35**, L04809, https://doi.org/10.1029/2007GL032165.

Kitzberger, T., P. M. Brown, E. K. Heyerdahl, T. W. Swetnam, and T. T. Veblen, 2007: Contingent Pacific–Atlantic Ocean influence on multicentury wildfire synchrony over western North America. *Proc. Natl. Acad. Sci. USA*, **104**, 543–548, https://doi.org/10.1073/pnas.0606078104.

Kochanski, A. K., D. V. Mallia, M. G. Fearon, J. Mandel, A. H. Souri, and T. Brown, 2019: Modeling wildfire smoke feedback mechanisms using a coupled fire-atmosphere model with a radiatively active aerosol scheme. *J. Geophys. Res. Atmos.*, **124**, 9099–9116, https://doi.org/10.1029/2019JD030558.

Labonne, M., F.-M. Breon, and F. Chevallier, 2007: Injection height of biomass burning aerosols as seen from a spaceborne lidar. *Geophys. Res. Lett.*, **34**, L11806, https://doi.org/10.1029/2007GL029311.

Landis, M., E. Edgerton, E. White, G. Wentworth, A. Sullivan, and A. Dillner, 2018: The impact of the 2016 Fort McMurray Horse River wildfire on ambient air pollution levels in the Athabasca Oil Sands region, Alberta, Canada. *Sci. Total Environ.*, **618**, 1665–1676, https://doi.org/10.1016/j.scitotenv.2017.10.008.

Lareau, N. P., and C. B. Clements, 2015: Cold smoke: Smoke-induced density currents cause unexpected smoke transport near large wildfires. *Atmos. Chem. Phys.*, **15**, 11 513–11 520, https://doi.org/10.5194/acp-15-11513-2015.

——, and ——, 2017: The mean and turbulent properties of a wildfire convective plume. *J. Appl. Meteor. Climatol.*, **56**, 2289–2299, https://doi.org/10.1175/JAMC-D-16-0384.1.

Littell, J. S., D. McKenzie, D. L. Peterson, and A. L. Westerling, 2009: Climate and wildfire area burned in western U.S. ecoprovinces, 1916–2003. *Ecol. Appl.*, **19**, 1003–1021, https://doi.org/10.1890/07-1183.1.

Lu, Z., W. Jun, X. Xu, X. Chen, S. Kondragunta, O. Torres, E. M. Wilcox, and J. Zeng, 2021: Hourly mapping of the layer height of thick smoke plumes over the western U.S. in 2020 severe fire season. *Front. Remote Sens.*, **2**, 36, https://doi.org/10.3389/frsen.2021.766628.

Lutsch, E., E. Dammers, S. Conway, and K. Strong, 2016: Long-range transport of NH_3, CO, HCN, and C_2H_6 from the 2014 Canadian wildfires. *Geophys. Res. Lett.*, **43**, 8286–8297, https://doi.org/10.1002/2016GL070114.

——, and Coauthors, 2019: Unprecedented atmospheric ammonia concentrations detected in the high Arctic from the 2017 Canadian wildfires. *J. Geophys. Res. Atmos.*, **124**, 8178–8202, https://doi.org/10.1029/2019JD030419.

Mattis, I., D. Müller, A. Ansmann, U. Wandinger, J. Preißler, P. Seifert, and M. Tesche, 2008: Ten years of multiwavelength Raman lidar observations of free-tropospheric aerosol layers over central Europe: Geometrical properties and annual cycle. *J. Geophys. Res.*, **113**, D20202, https://doi.org/10.1029/2007JD009636.

Meng, J., and Coauthors, 2019: Source contributions to ambient fine particulate matter for Canada. *Environ. Sci. Technol.*, **53**, 10 269–10 278, https://doi.org/10.1021/acs.est.9b02461.

Müller, D., I. Mattis, U. Wandinger, A. Ansmann, D. Althausen, and A. Stohl, 2005: Raman lidar observations of aged Siberian and Canadian forest fire smoke in the free troposphere over Germany in 2003: Microphysical particle characterization. *J. Geophys. Res.*, **110**, D17201, https://doi.org/10.1029/2004JD005756.

Peterson, D. A., E. J. Hyer, J. R. Campbell, M. D. Fromm, J. W. Hair, C. F. Butler, and M. A. Fenn, 2015: The 2013 Rim fire: Implications for predicting extreme fire spread, pyroconvection, and smoke emissions. *Bull. Amer. Meteor. Soc.*, **96**, 229–247, https://doi.org/10.1175/BAMS-D-14-00060.1.

Raffuse, S. M., K. J. Craig, N. K. Larkin, T. T. Strand, D. C. Sullivan, N. J. M. Wheeler, and R. Solomon, 2012: An evaluation of modeled plume injection height with satellite-derived observed plume height. *Atmosphere*, **3**, 103–123, https://doi.org/10.3390/atmos3010103.

Sharman, R. D., L. B. Cornman, G. Meymaris, J. Pearson, and T. Farrar, 2014: Description and derived climatologies of automated in situ eddy-dissipation-rate reports of atmospheric turbulence. *J. Appl. Meteor. Climatol.*, **53**, 1416–1432, https://doi.org/10.1175/JAMC-D-13-0329.1.

Val Martin, M., J. A. Logan, R. A. Kahn, F.-Y. Leung, D. L. Nelson, and D. J. Diner, 2010: Smoke injection heights from fires in North America: Analysis of 5 years of satellite observations. *Atmos. Chem. Phys.*, **10**, 1491–1510, https://doi.org/10.5194/acp-10-1491-2010.

——, R. A. Kahn, J. A. Logan, R. Paugam, M. Wooster, and C. Ichoku, 2012: Space-based observational constraints for 1-D fire smoke plume-rise models. *J. Geophys. Res.*, **117**, D22204, https://doi.org/10.1029/2012JD018370.

Viegas, D. X., 1998: Convective processes in forest fires. *Buoyant Convection in Geophysical Flows*, E. J. Plate et al., Eds., Springer, 401–420.

Wandinger, U., and Coauthors, 2002: Optical and microphysical characterization of biomass-burning and industrial-pollution aerosols from multiwavelength lidar and aircraft measurements. *J. Geophys. Res.*, **107**, 8125, https://doi.org/10.1029/2000JD000202.

Westerling, A. L., 2016: Increasing western US forest wildfire activity: Sensitivity to changes in the timing of spring. *Philos. Trans. Roy. Soc. London*, **371B**, 20150178, https://doi.org/10.1098/rstb.2015.0178.

Ye, X., and Coauthors, 2021: Evaluation and intercomparison of wildfire smoke forecasts from multiple modeling systems for the 2019 Williams Flats fire. *Atmos. Chem. Phys.*, **21**, 14 427–14 469, https://doi.org/10.5194/acp-21-14427-2021.

Youn, D., and Coauthors, 2011: Impacts of aerosols on regional meteorology due to Siberian forest fires in May 2003. *Atmos. Environ.*, **45**, 1407–1412, https://doi.org/10.1016/j.atmosenv.2010.12.028.

Zheng, Y., J. Liu, H. Jian, X. Fan, and F. Yan, 2021: Fire diurnal cycle derived from a combination of the Himawari-8 and VIIRS satellites to improve fire emission assessments in southeast Australia. *Remote Sens.*, **13**, 2852, https://doi.org/10.3390/rs13152852.